

Enhancing Surgical Accuracy Using Virtual Fixtures and Motion Compensation in Robotic Beating Heart Surgery*

G. P. Moustris, A. I. Mantelos, and C. S. Tzafestas

Abstract—This paper proposes a novel technique for applying virtual fixtures in a changing environment. The main targeted application is robotic beating heart surgery, which enables the surgeon to operate directly on a beating heart. Using a motion compensation framework, the motion of the heart surface is stabilized in a virtual space, which is presented to the surgeon to operate in. Consequently, the fixture is implemented in this static space, bypassing problems of dynamic fixtures such as position update, placement and force transients. Randomized experiments were performed using a trained surgeon comparing our approach to simple motion compensation and no compensation at all. The positive effect of the fixture in surgical accuracy for a tracking task is also discussed.

I. INTRODUCTION

THE introduction of robots in minimally invasive surgery (MIS) has been met with enthusiasm from medical practitioners, since it offers significant advantages such as high dexterity, stable imaging, stereo vision, tremor filtering and higher precision, to name a few. The typical setup employs a master-slave system, where the surgeon teleoperates the robotic slave manipulators sitting at a master console. However, one of the major shortcomings is the lack of haptic feedback, either tactile or force. This hinders the full utilization of the robot capabilities, and introduces further delays in the learning curve since surgeons consider haptic display a major advantage, especially when complex surgical tasks are performed, e.g. suturing, knot tying etc. Several studies have measured the positive effect of haptic feedback in robotic surgery as well as in training young surgeons using virtual reality MIS simulators [1–5].

Force feedback can be used to augment and extend surgical ability by providing sensorial cues, escaping from a mere force reflection from the slave to the master console. This is most prominently demonstrated in the use of virtual fixtures (VF), which affect the robot motion either constraining it to move in a designated space (forbidden-zone VF) or guiding it to a specified path/trajectory (guidance VF). The fixture can be considered as an invisible ruler which exerts forces to the master console, either

repelling or attracting, according to some force law. Virtual fixtures have already been investigated in various robotic surgery scenarios [6–9], showing a positive effect on motion accuracy and task completion time. However, most of these applications only consider static fixtures, applied to environments which do not present deformation. This excludes important interventions such as off-pump coronary artery bypass graft surgery (OPCAB). Typically in coronary artery bypass graft surgery (CABG), the patient undergoes cardiopulmonary bypass (CPB), and is connected to the heart-lung machine to stop the heart from beating. The surgeon consequently operates on the still heart. To prevent arresting the heart, in OPCAB the surgeon operates directly on the beating heart, without the use of CPB. However, mechanical or vacuum stabilizers are placed on the surgical field (myocardium), reducing the heart motion. Even though OPCAB has been shown to have significant positive effects on the patient, the stress induced by the stabilizers on the heart can cause hemodynamic disorders [10]. Furthermore, there is also a residual motion in the field since the stabilizers do not cancel the motion entirely.

Motion compensation has allowed for operating directly on the beating heart i.e. the so called *robotic beating-heart surgery*. This refers to the apparent cancellation of organ motion in the surgical field through image processing and robot control. Typically, the motion of the surgical field (e.g. heart beat, respiratory motion etc) is captured by an imaging device in real-time, is rectified, and presented to the surgeon as still. Concurrently, the robot maintains a steady pose with respect to the field, essentially tracking its motion and moving along with it. This function however, is transparent to the surgeon on the master console, who effectively operates on a static image without perceiving the motion of the slave robot.

Robotic motion compensation presents a significant advantage for OPCAB since it obviates the need for stabilizers. The control scheme falls under the shared control paradigm as both the controller and the surgeon use the robot at the same time. Motion compensation generally involves three main tasks; mechanical synchronization, image stabilization and shared control. One of the first applications of motion compensation referred to cardiac surgery [11] where the notion of heartbeat synchronization was introduced. Motion estimation and Model Predictive Controllers [12–14] have also been applied, mainly due to the fast dynamics of the heart surface. Other modalities such

*The work leading to these results has received funding by the European Union under project MOBOT with grant FP7-ICT-2011-9-600796.

G. P. Moustris, A. I. Mantelos., and C. S. Tzafestas are with the School of Electrical & Computer Engineering, National Technical University of Athens, Intelligent Robotics & Automation Laboratory, Zographou Campus, Athens, GR 15773 (phone: +30-210-7721527, fax:+30-210-7722489, e-mails: {gmoustri@mail, mantelos@cc.ece, ktzaf@cs}.ntua.gr)

as ultrasound [15,16] and forces sensors [17] have also been presented. Image rectification and stabilization algorithms for motion compensation are presented in [18–21].

The application of dynamic VFs in cardiac surgery presents two problems; the first is the placement of the fixture itself. Apparently, as the environment moves, the fixture must be recalculated in real-time and repositioned in order to reflect the current situation. This cannot be trivially performed, especially in forbidden-zone VFs, as the deformation may result from the interaction of the environment with the robot; for instance, the manipulator could deform a tissue and essentially be placed beyond the fixture where no force is applied. The second problem regards the haptic perception of the dynamic fixture. Since the VF changes shape following the environment deformation, the applied force depends not only on the robot position but the fixture position relative to the robot. Thus, the exerted forces will present transients which may confuse the surgeon, especially if the environment changes continuously e.g. heart.

Dynamic VFs for cardiac surgery have been discussed in [22] where the authors distinguished two ways on fixture placement; one depending on the predicted position of the VF, based on a largely periodic environment movement, and the second based on the current environment position. The study focused on the first case, placing fixtures on a heart surface mockup. Experiments showed a consistent increase in precision and decrease of the user applied force. A dynamic guidance VF for intercardiac surgery has been demonstrated in [23]. The authors combined real-time MRI to model the motion inside the left ventricle, and computed the access reference path on-the-fly. Two VFs were examined; one based on a simple linear spring, and; a second one that allowed the surgeon to move freely when close to the fixture. Experiments using prerecorded MRI sequences showed a decrease in the offset error from the reference. This work was expanded in [24] where forbidden zone VFs were used instead.

In this work we present a novel way of applying virtual fixtures for beating heart surgery, utilizing a new motion compensation framework under which the mechanical synchronization, the image stabilization and the shared control emerge and combine naturally[25]. This is achieved by using the Strip-Wise Affine Map (SWAM) [26], which shifts the control to a stabilized canonical space where the robot and the image are still. Concurrently, the VF is placed in the stabilized space, which is presented to the surgeon as static, thus avoiding the problem of transient forces and fixture replacement. The fixture aims to help the surgeon guide the robot for a simple tracking task on the heart, following a predefined curve.

I. THEORETICAL FRAMEWORK

A. Preliminary Concepts

A typical setup for motion compensation in robotic cardiac surgery is shown in Fig. 1. The surgical field is manipulated by the slave robot and overviewed by an endoscopic camera. This camera image will be called the “physical image”. Reference features are extracted from the image and used in subsequent tasks. The physical image is then rectified and presented to the surgeon, who sits on the master console operating the controls. The stabilized image will be called the “canonical image”. The surgeon perceives the surgical field in the canonical image as still, and produces the human input which is combined with the reference signal by the shared controller. Closing the loop, the shared control signal is fed to the slave robot.

We identify three spaces attached to each subsystem; the *physical world space* W_p i.e. the Cartesian space where the slave robot and surgical field dwell; the *physical image space* I_p , denoting the image space of the world space through the camera, and; the *canonical image space* I_c , which is the rectified image space where the physical image is still. The three spaces are related by two transformations. Specifically, $P:W_p \rightarrow I_p$, $P \in GPL(W_p)$ is the projective transformation involving the camera matrix. For simplicity, in this work the pinhole camera model is used. The canonical and physical images are related by a non-linear rectification map $\Psi: I_p \rightarrow I_c$ which must be bijective in order to prevent unnatural distortions of the surgical field presented to the surgeon.

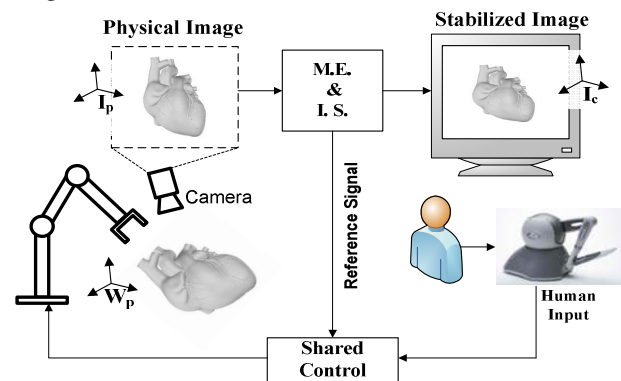


Fig.1. Typical setup for motion compensation in robotic cardiac surgery

The system tracks the motion of a *reference manifold* $M_p(u,t)$ in the surgical field. For example, M_p could be a point on the heart surface (0-manifold), a line (1-manifold) or a patch (2-manifold). For the mechanical synchronization task, the goal is to maintain a fixed pose to the reference manifold. Specifically, let $T_S(\tau_s)$ be a frame rigidly attached to the slave robot tool, expressing the pose with respect to the world frame W_p . We denote the position of T_S as ${}^p q_s$. The vector τ_s is the robot input. Also, let $T_G(t)$ be a frame of a goal pose on the reference manifold at point $q_G(t)$. T_G depends on time since the reference manifold changes shape due to cardiac pulsation. R_G is the *goal orientation* and q_G is

the *goal point* in M_p . The general synchronization problem asks for the input τ , such that the frames remain fixed to each other. A simpler version of the problem is to consider only the Cartesian position (i.e. only q_G), and ignore the rotational part. This reduces to a Cartesian tracking problem.

Regarding the image stabilization task, let F_p be the physical image of the field through the camera, and $IM_p = P(M_p)$ be the image of the reference manifold. Formally, F_p is a function from I_p to some color space and IM_p is a subset of $dom(F_p)$. F_p is mapped to the canonical image space through Ψ , i.e. $dom(F_c) = \Psi(dom(F_p); IM_p)$. Similarly $IM_c = \Psi(IM_p)$, $IM_c \subset dom(F_c) \subset I_c$ is the reference manifold in the canonical image. Note that Ψ is not a static transformation but depends on IM_p as a parameter. This is natural since the purpose of image stabilization is to map the physical image to the canonical image in such a way that the reference manifold in the physical image is mapped to a *fixed* sub-domain in I_c i.e. to IM_c . However since IM_p deforms through time, Ψ must depend on the actual IM_p at each instance. In the general case where the robot's pose is considered, the entire robot image block must be transformed in order to stabilize the orientation as well as the position. In the simpler case of Cartesian synchronization, only the robot's position in the image must be compensated.

In this work we consider the Cartesian compensation problem for a planar I -manifold reference i.e. a planar curve. The canonical reference manifold IM_c is a fixed straight line in the canonical image. Thus, the physical curve is always mapped to a straight line. In such a case, if the surgeon wants to cut along a curve on the pulsating heart, the task is reduced to tracking a static straight line in the canonical image.

To produce the motion synchronization and image stabilization algorithms, we introduce the *canonical world space* W_c , which is a Cartesian 3D space containing the stabilized robot and reference manifold. The physical and canonical world spaces are related by the bijective map $\Phi: W_c \rightarrow W_p$, as seen in the commutative diagram of Fig. 2. The control of the robot takes place in the canonical world space, where the reference manifold M_c is a straight line. Essentially the surgeon operates in W_c looking at its image in I_c .

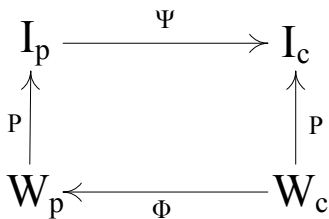


Fig. 2. Commutative diagram relating the four spaces and transformations

From the diagram, it can be verified that $\Psi = P \circ \Phi^{-1} \circ P^{-1}$. The inverse projective map P^{-1} exists because the reference manifold lays on the plane $z=0$. The map Φ is an extended version of the strip-wise affine map, analyzed in the

following section.

B. Strip-Wise Affine Map

The strip-wise affine map (SWAM) is a piecewise linear homeomorphism between two spaces. It acts by inducing a strip decomposition on the x - y plane and then applying an affine map between them. It has been successfully applied to mobile robot tracking control since it reduces path tracking to straight line tracking [27,28]

The map takes a *polygonal line* from the physical space, and maps it to the x_c -axis in the canonical space. This fits well into the control as the reference manifold is extracted from the physical image and projected to the physical space as a collection of points, rather than a smooth curve. Thus let $\{w_i\}$, $i=1..n$, $w_i = ({}^p x_i, {}^p y_i, 0)$ be the vertices of the polygonal line, lying on the plane $z=0$. Each vertex is projected to a point a_i on the real axis in the canonical world according to its normalized length. Furthermore, let $q_p = (x_p, y_p, z_p)$ be a point in W_p and $q_c = (x_c, y_c, z_c)$ a point in W_c . The SWAM maps q_c to q_p under the equation,

$$q_p = \begin{bmatrix} x_p \\ y_p \\ z_p \end{bmatrix} = \begin{bmatrix} y_c S \cos \theta_s + f_x(x_c) \\ y_c S \sin \theta_s + f_y(x_c) \\ z_c \end{bmatrix} = \Phi(q_c) \quad (1)$$

where θ_s is some angle, called the *shifting angle*. The functions f_x and f_y are given by,

$$f_x(x_c) = \sum_{k=0}^n [{}^p x_k + S \cdot (x_c - a_k) \cos \theta_k] \psi_k, \quad (2)$$

$$f_y(x_c) = \sum_{k=0}^n [{}^p y_k + S \cdot (x_c - a_k) \sin \theta_k] \psi_k$$

The angles θ_k are the angles of each edge $[w_k w_{k+1}]$ with respect to the physical x -axis, and $\psi_k(x_c)$ is a unit rectangle pulse function in W_c with support set $[a_k, a_{k+1})$. Observe that (2) is a piece-wise linear parameterization of the reference manifold such that $M_p = (f_x, f_y, 0)$, and thus x_c is the coordinate parametrizing it. Equations (1),(2) show that if the robot moves on a vertical plane parallel to the x_c -axis in the canonical space, its image in the physical space moves parallel to the reference manifold by a standard offset $g = (y_c S \cos \theta_s, y_c S \sin \theta_s, z_c)$ from point $(f_x(x_c), f_y(x_c), 0)$ laying on M_p . Defining the goal point as,

$$q_G(x_c) = [f_x(x_c) \quad f_y(x_c) \quad 0]^T \quad (3)$$

then (1) takes the compact form,

$$q_p = g(y_c, z_c) + q_G(x_c) \quad (4)$$

Using the SWAM the control of the robot is transferred to the canonical world where the objective for the surgeon is to track the x_c -axis. Using this map as a basis, the virtual fixture can be placed in the canonical space, as described in the following section.

II. VIRTUAL FIXTURE

Let W_m be the Cartesian physical space at the master console. To bind the master and slave systems we identify W_m with W_c , up to a scaling factor on the x - y plane. Thus, if ${}^p q_m = ({}^p x_m, {}^p y_m, {}^p z_m)$ is the position of the master robot in W_m and ${}^c q_m = ({}^c x_m, {}^c y_m, {}^c z_m)$ its projection in W_c , then $({}^c x_m, {}^c y_m, {}^c z_m) = (L^p x_m, L^p y_m, {}^p z_m)$, where L is some real constant. In a similar fashion let ${}^p q_s$ be the physical position of the slave robot in W_p , and ${}^p q_r$ be the physical image of a reference point (Fig. 3).

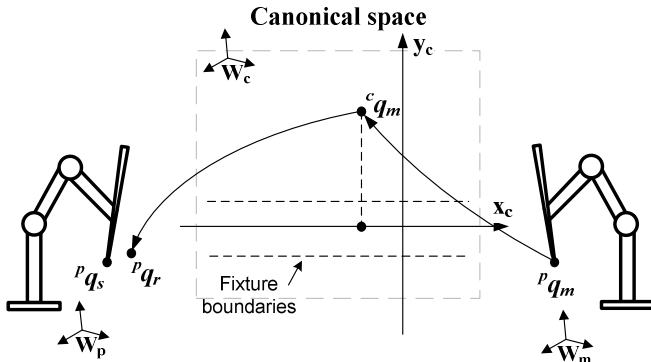


Fig. 3. Definition of the robot and reference images in the physical and canonical spaces.

The goal of the slave robot is to follow the physical reference point ${}^p q_r$. In this work we have used a simple PID controller to perform this task. The reference point is the projection of the canonical master position in W_p i.e. ${}^c q_r \equiv {}^c q_m$. The 3D VF is placed in the canonical space, around the x_c -axis and attracts the master towards the line. It exerts a force perpendicular to x_c , thus the surgeon is free to move about the x_c -axis but experiences an attractive force only in a direction pointing towards x_c . The fixture is defined in a cylinder, with external radius ε . placed at the x_c -axis. Two more internal cylinders are also defined. One with radius $\beta < \varepsilon$ and a second one with radius $\delta < \beta$ (Fig. 4). These areas define a force profile that starts linearly from ε to β , exerts a constant force between δ and β , falling back linearly to zero. The vectorial force lies on the $z_c y_c$ plane, pointing towards x_c .

If the canonical position of the master robot is at point p , let \mathbf{r} be the component of the position vector in $z_c y_c$. Furthermore, let φ be the angle between \mathbf{r} and the z_c axis. Then, the unit force vector is defined by,

$$\mathbf{u}_F = [0, -\sin \varphi, -\cos \varphi]^T \quad (5)$$

Thus, the fixture force is defined by the following formula,

$$\mathbf{F}_{VF} = |F_{VF}| \mathbf{u}_F \quad (6)$$

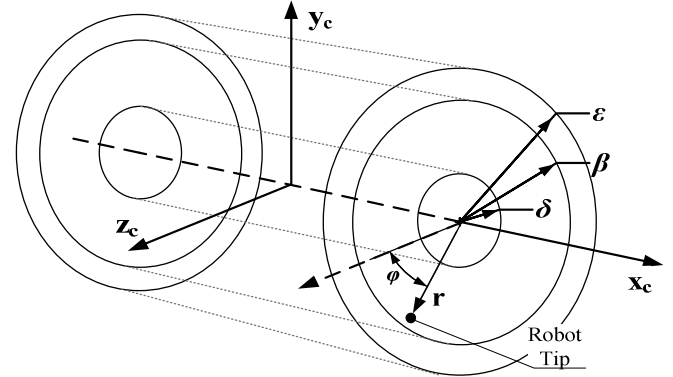


Fig. 4. Definition of the fixture about the canonical x_c -axis. The fixture is contained in the cylinder with radius ε . Internal cylinders (δ, β) define different force profiles.

The magnitude $|F_{VF}|$ of the force vector, is given by,

$$|F_{VF}(r)| = \begin{cases} 0 & , \varepsilon \leq r \\ F_{\max}(r - \varepsilon) / (\beta - \varepsilon) & , \beta \leq r < \varepsilon \\ F_{\max} & , \delta \leq r < \beta \\ F_{\max} r / \delta & , 0 \leq r < \delta \end{cases} \quad (7)$$

where F_{\max} is the maximum fixture force and $r = |\mathbf{r}|$. The force profile can be seen in the following diagram.

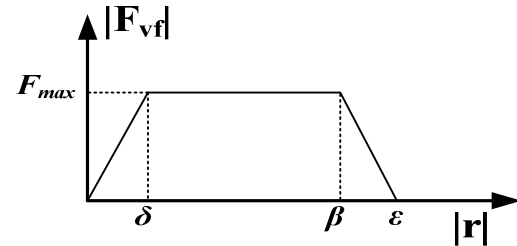


Fig. 5. Force profile of the virtual fixture according to the distance from the canonical axis.

The guidance fixture has been contained in the cylinder in order to prevent an unwanted drag effect in the entire surgical field, which would deter the surgeon from moving in different areas. Note that in the inner cylinder, the force diminishes linearly to zero. This has been selected in order to allow the surgeon to perform the surgical task when guided to the reference path. In a different situation e.g. if the force was present at $r=0$, normal positional errors of the surgeon due to tremor or the inherent limited accuracy of humans, would result in switching forces being applied, as the tip would “wobble” about the axis. This would have a rather undesirable effect since the fixture would be too stiff, not allowing the surgeon to perform motion in the force direction. Thus a spring was inserted, in order to present

haptic cues to the user and not confine him/her in the inner tube.

III. IMPLEMENTATION

The master-slave system consists of the PHANToM Omni and Desktop for the master-slave sides respectively. The robots have identical mechanical structure, with DC motor actuators for the first three joints. The Tool Center Point (TCP) is located at the intersection of the last three joints that form the gimbal. Since only Cartesian compensation is considered, utilizing the first three joints, the gimbal was locked and rigidly attached to the second link in each robot.

To simulate a lancet on the Slave robot, a metallic needle was attached to the gimbal stylus (see Fig. 6), mirroring a similar metallic tip on the master. The robots were calibrated using checkerboards, which also defined the physical and canonical world frames. In front of the slave robot lays a semi-transparent screen, defining the surgical field. Underneath, there is a projector showing the reference line on the screen. The surgeon views the field through a pole-mounted camera, which was calibrated and registered to W_p

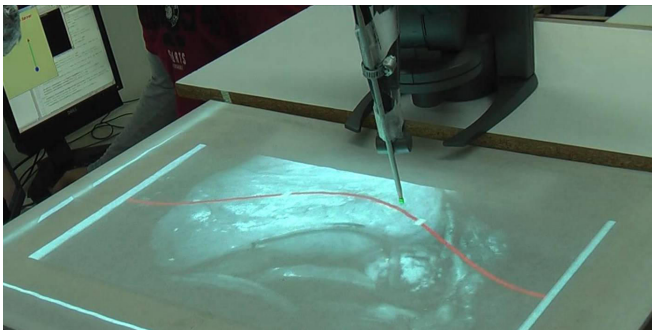


Fig. 6. View of the slave robot and the surgical field. The robot tracks a red line on a heart image projected onto a semi-transparent screen from a projector underneath the screen.

In order to reduce the computational overhead and latency of the system, the robots were connected to two different computers while the camera was feeding the input to a third. The system runs in three parallel loops, distributed across the three computers; the Servo loop; the Graphics loop and; the Communications loop.

The servo loop, operating at 1 KHz, controls the slave robot querying its configuration and implementing the PID controller for the tracking of the reference position, setting the forces on the first three joints. The PID follows the update rate of the communication loop (100 Hz) since all three loops are asynchronous. On the master side, a similar servo loop also applies the force feedback to the surgeon console, at a 1 KHz update rate. The Graphics loop performs the image acquisition and rectification on the master console. It acquires the camera image, processes it and presents it to the surgeon stabilized. The loop was runs in MATLAB and OpenCV, achieving a refresh rate of approximately 30Hz. To speed up the computation, the image resolution was reduced to 320x240 pixels and converted to grayscale, following the

detection of the red reference line. The graphics loop essentially applies the Ψ transform on the physical image.

Finally, the communications loop utilizes UDP sockets at an update rate of 100 Hz. Since UDP lacks an error correction mechanism, the data packets were framed with a predefined header to detect corruption.

IV. EXPERIMENTAL RESULTS

Experiments were designed in order to test the effect of haptic feedback, against simple compensation with no feedback and no compensation at all. A trained surgeon was asked to operate the master console, in order to perform a tracking task on a pulsating red line embedded into an endoscopic image of the heart. Specifically, two white square markers were placed on each side of the line. The task of the surgeon was to start from the left marker, follow the line and touch the right marker, then go back to the original marker. This was to be performed two times overall.

The entire image was deformed according to the reference line in order to give the impression of a beating heart. The line followed a periodic movement, driven by a pre-recorder ECG signal set to three frequencies. To capture the robot motion, a green marker was attached to the needle tip. Overlooking the scene was a HD camera recording the experiment in 1080p resolution. Prior to the experiments both the surgeon's and the HD camera were calibrated and registered to the physical world frame.

The experimental trials consisted of three groups (no compensation, simple compensation, compensation with VF). Each group, in turn, comprised three frequency groups according to heart rate (12 bmp, 15 bmp, 18 bmp). For each frequency, four experimental trials were performed. Thus, the number of all trials was $3 \times 3 \times 4 = 36$. The trials were fully randomized using a discrete uniform distribution. Each trial was removed from the pool in subsequent runs. The VF parameters were set to $\varepsilon=40\text{mm}$, $\beta=30\text{mm}$, $\delta=5\text{mm}$. The maximum force was $F_{max}=1\text{N}$. In the case of the first group (no compensation) the surgeon viewed the un-rectified physical image, while in the next two groups viewed the rectified image (Fig. 7 left and right respectively.).

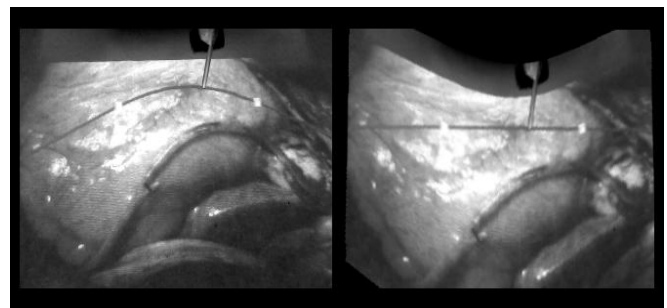


Fig. 7. View of the surgical field through the camera. (Left) Physical image. (Right) Canonical image. The slave robot is visible in both images. The white markers can also be distinguished.

The slave robot's tip movement was extracted in post-processing from the HD camera video using a color filter in

each frame to extract the tip's green marker, as well as the red line. Following, the pixel trajectory was filtered to reduce noise and back-projected to the Cartesian space to perform the analysis.

To assess the effect of the virtual fixtures, the error distance of the tip to the line was calculated for each frame and a statistical analysis was performed. In Fig. 8 the aggregate box plot per group and frequency is presented. Since each trial is different in length (time), the averages were used. Thus, each box shows the distribution of the four means for the respective trials in each frequency.

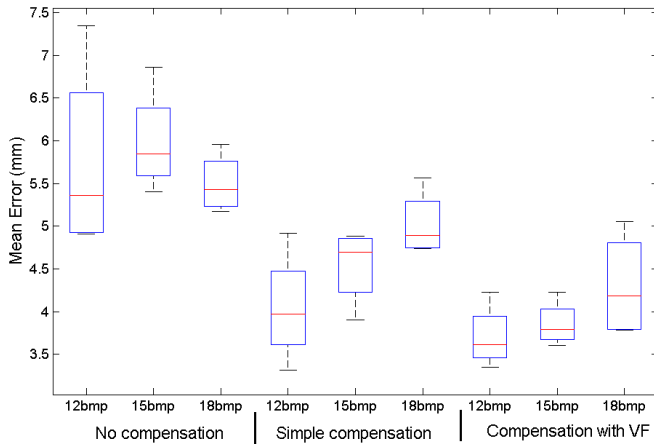


Fig. 8 Box plot of mean error distance from the reference path, according to frequency and group.

A summary of the statistical results of the groups, according to frequency, is presented in Table I.

TABLE I
STATISTICAL RESULTS FOR EACH GROUP PER FREQUENCY

	12bpm	15bpm	18bpm	group
mean (mm)	5.743	5.987	5.496	NC ^a
mean (mm)	4.042	4.544	5.020	SC ^b
mean (mm)	3.700	3.850	4.302	VF ^c

^aNo Compensation, ^bSimple Compensation, ^cCompensation with Virtual Fixtures

Table I shows an increase in the average error across frequencies, for the last two groups. This can be attributed to the specific implementation of the proposed algorithm since the current h/w capabilities limit the *bmp* that can be processed in real time. Indeed, it was experimentally confirmed that frequencies beyond 20bpm were not capable of being processed in real-time by our hardware, injecting significant delays into the control loop. Even so, the VF group presents a systematic decrease of the average error across the three frequencies, compared to the other groups. It is also worth noting that the error increase in the VF group is smaller i.e. the VF also compensates for the errors due to frequency.

The comparison of the results according to the three groups is shown in Fig. 9. Each box expresses the

distribution of the twelve means of the respective trials, for each group. The statistics for the aggregate results are presented in Table II.

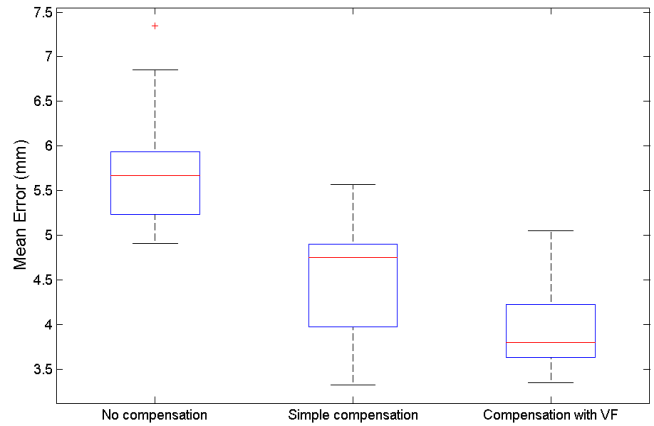


Fig. 9. Box plot for the experiments, aggregated over the three groups.

TABLE II
AGGREGATE RESULTS FOR THE THREE GROUPS

	NC	SC	VF
mean (mm)	5.742	4.535	3.951
Rel.Diff. ^a	-	-21.01%	-12.88%
Std.	0.733	0.623	0.483
Rel.Diff. ^b	-	-15.00%	-22.50%

^aRelative difference between consecutive means. ^bRelative difference between consecutive standard deviations

Table II shows a decrease of the average mean error for the virtual fixture group. Quantitatively, VFs decrease the average error by 12.88% with respect to the simple compensation group and by 31.19% with respect to no compensation at all. Furthermore, the standard deviation of the means distribution is also decreased by 22.5% w.r.t. simple compensation and 34.1% w.r.t. no compensation. This implies that the virtual fixture enables the surgeon to consistently follow the predefined reference with better accuracy and small perturbations. The residual error in the VF group can be attributed to the surgeon's inherent accuracy, as well as the experimental errors inserted by the delay of the graphics loop.

These preliminary results show the promise of our approach and seem to validate the hypothesis that haptic assistance in robotic beating heart surgery presents advantages for the surgeon, in terms of accuracy. Although the number of experimental subjects is very small, further studies using a bigger pool of surgeons are expected to clearly show this advantage.

V. CONCLUSION AND FUTURE WORK

We have presented a novel framework for applying dynamic virtual fixtures in robotic beating heart surgery, employing motion compensation. In this way, the problems

regarding the dynamic nature of the fixtures e.g. placement and force transients, are mitigated since the VF is placed in a static space provided by the motion compensation algorithm. Randomized experiments, across various heart rates, showed the feasibility of our approach and a systematic positive effect of the VF in surgical accuracy. Future work will focus on extending our approach to more complex tasks which could significantly augment various stages of surgery e.g. knot tying and suturing.

REFERENCES

- [1] B.T. Bethea, A.M. Okamura, M. Kitagawa, T.P. Fitton, S.M. Cattaneo, V.L. Gott, W.A. Baumgartner, and D.D. Yuh, "Application of haptic feedback to robotic surgery," *Journal of laparoendoscopic & advanced surgical techniques. Part A*, vol. 14, Jun. 2004, pp. 191–195.
- [2] M.K. Chmarra, J. Dankelman, J.J. van den Dobbelen, and F.-W. Jansen, "Force feedback and basic laparoscopic skills," *Surgical Endoscopy*, vol. 22, Oct. 2008, pp. 2140–2148.
- [3] P. Ström, L. Hedman, L. Särnå, A. Kjellin, T. Wredmark, and L. Felländer-Tsai, "Early exposure to haptic feedback enhances performance in surgical simulator training: a prospective randomized crossover study in surgical residents," *Surgical endoscopy*, vol. 20, Sep. 2006, pp. 1383–1388.
- [4] G. Tholey, J.P. Desai, and A.E. Castellanos, "Force Feedback Plays a Significant Role in Minimally Invasive Surgery," *Annals of Surgery*, vol. 241, Jan. 2005, pp. 102–109.
- [5] O.A.J. van der Meijden and M.P. Schijven, "The value of haptic feedback in conventional and robot-assisted minimal invasive surgery and virtual reality training: a current review," *Surgical Endoscopy*, vol. 23, Jun. 2009, pp. 1180–1190.
- [6] M. Li, A. Kapoor, and R.H. Taylor, "Telerobotic Control by Virtual Fixtures for Surgical Applications," *Advances in Telerobotics*, M. Ferre, M. Buss, R. Aracil, C. Melchiorri, and C. Balaguer, eds., Springer Berlin Heidelberg, 2007, pp. 381–401.
- [7] M. Li and R.H. Taylor, "Spatial motion constraints in medical robot using virtual fixtures generated by anatomy," *Proc. of the IEEE Int. Conf. on Robotics and Automation*, New Orleans, LA, USA, May 2004, pp. 1270 – 1275 Vol.2.
- [8] M. Li and R.H. Taylor, "Performance of Surgical Robots with Automatically Generated Spatial Virtual Fixtures," *Proc. of the IEEE Int. Conf. on Robotics and Automation*, Barcelona, Spain, April 2005, pp. 217 – 222.
- [9] S. Park, R. Howe, and D. Torchiana, "Virtual Fixtures for Robotic Cardiac Surgery," *Medical Image Computing and Computer-Assisted Intervention – MICCAI 2001*, W. Niessen and M. Viergever, eds., Springer Berlin Heidelberg, 2001, pp. 1419–1420.
- [10] P.P.M. de Oliveira, D.M. Braile, R.W. Vieira, O. Petrucci Junior, L.M. Silveira Filho, K.A. de S. Vilarinho, E.S. de O. Barbosa, and N. Antunes, "Hemodynamic disorders related to beating heart surgery using cardiac stabilizers: experimental study," *Revista brasileira de cirurgia cardiovascular: órgão oficial da Sociedade Brasileira de Cirurgia Cardiovascular*, vol. 22, Dec. 2007, pp. 407–415.
- [11] Y. Nakamura, K. Kishi, and H. Kawakami, "Heartbeat synchronization for robotic cardiac surgery," *Proc. of the IEEE Int. Conf. on Robotics and Automation*, Seoul, Korea, May 2001, pp. 2014–2019 vol.2.
- [12] J. Gangloff, R. Ginhoux, M. de Mathelin, L. Soler, and J. Marescaux, "Model predictive control for compensation of cyclic organ motions in teleoperated laparoscopic surgery," *Control Systems Technology, IEEE Transactions on*, vol. 14, 2006, pp. 235–246.
- [13] R. Ginhoux, J. Gangloff, M. de Mathelin, L. Soler, M.M.A. Sanchez, and J. Marescaux, "Active filtering of physiological motion in robotized surgery using predictive control," *Robotics, IEEE Transactions on*, vol. 21, 2005, pp. 67–79.
- [14] O. Bebek and M.C. Cavusoglu, "Predictive control algorithms using biological signals for active relative motion canceling in robotic assisted heart surgery," *Proc. of the IEEE Int. Conf. on Robotics and Automation*, Orlando, Florida, USA, May 2006, pp. 237–244.
- [15] S. Yuen, S. Kesner, N. Vasilyev, P. Del Nido, and R. Howe, "3D Ultrasound-Guided Motion Compensation System for Beating Heart Mitral Valve Repair," *Medical Image Computing and Computer-Assisted Intervention*, New York, NY 2008, pp. 711–719.
- [16] S.B. Kesner and R.D. Howe, "Design and control of motion compensation cardiac catheters," *Proc. of the IEEE Int. Conf. on Robotics and Automation*, Anchorage, Alaska, USA May 2010, pp. 1059–1065.
- [17] B. Cagneau, N. Zemiti, D. Bellot, and G. Morel, "Physiological Motion Compensation in Robotized Surgery using Force Feedback Control," *Proc. of the IEEE Int. Conf. on Robotics and Automation*, Roma, Italy, April 2007, pp. 1881–1886.
- [18] P. Mountney and G.-Z. Yang, "Soft Tissue Tracking for Minimally Invasive Surgery: Learning Local Deformation Online," *Medical Image Computing and Computer-Assisted Intervention – MICCAI 2008*, D. Metaxas, L. Axel, G. Fichtinger, and G. Székely, eds., Springer Berlin / Heidelberg, 2008, pp. 364–372.
- [19] D. Stoyanov, G.P. Mylonas, F. Deligianni, A. Darzi, and G.Z. Yang, "Soft-Tissue Motion Tracking and Structure Estimation for Robotic Assisted MIS Procedures," *Medical Image Computing and Computer-Assisted Intervention – MICCAI 2005*, J. Duncan and G. Gerig, eds., Springer Berlin / Heidelberg, 2005, pp. 139–146.
- [20] R. Richa, A.P.L. Bó, and P. Poignet, "Towards robust 3D visual tracking for motion compensation in beating heart surgery," *Medical Image Analysis*, vol. 15, Jun. 2011, pp. 302–315.
- [21] D. Stoyanov and G.-Z. Yang, "Stabilization of Image Motion for Robotic Assisted Beating Heart Surgery," *Medical Image Computing and Computer-Assisted Intervention – MICCAI 2007*, N. Ayache, S. Ourselin, and A. Maeder, eds., Springer Berlin / Heidelberg, 2007, pp. 417–424.
- [22] T.L. Gibo, L.N. Verner, D.D. Yuh, and A.M. Okamura, "Design considerations and human-machine performance of moving virtual fixtures," *Proc. of the IEEE Int. Conf. on Robotics and Automation*, Kobe, Japan, May 2009, pp. 671 –676.
- [23] N.V. Navkar, Z. Deng, D.J. Shah, K.E. Bekris, and N.V. Tsekos, "Visual and force-feedback guidance for robot-assisted interventions in the beating heart with real-time MRI," *Proc. of the IEEE Int. Conf. on Robotics and Automation*, St. Paul, Minnesota, USA, May 2012, pp. 689 –694.
- [24] N. Navkar, Z. Deng, D. Shah, and N. Tsekos, "A Framework for Integrating real-time MRI with Robot Control: Application to Simulated Transapical Cardiac Interventions," *IEEE Transactions on Biomedical Engineering*, vol. PP, 2012, p. 1.
- [25] G.P. Moustris, A.I. Mantelos, and C.S. Tzafestas, "Shared Control for Motion Compensation in Robotic Beating Heart Surgery," *Proc. of the IEEE Int. Conf. on Robotics and Automation*, Karlsruhe, Germany, May 2013.
- [26] G. Moustris and S.G. Tzafestas, "Reducing a class of polygonal path tracking to straight line tracking via nonlinear strip-wise affine transformation," *Mathematics and Computers in Simulation*, vol. 79, Nov. 2008, pp. 133–148.
- [27] G.P. Moustris and S.G. Tzafestas, "Switching fuzzy tracking control for mobile robots under curvature constraints," *Control Engineering Practice*, vol. 19, Jan. 2011, pp. 45–53.
- [28] G.P. Moustris, K.M. Deliparaschos, and S.G. Tzafestas, "Feedback equivalence and control of mobile robots through a scalable FPGA architecture," *Recent Advances in Mobile Robotics*, A.V. Topalov, ed., InTech, 2011, pp. 401–426.